Coassembly of exfoliated Ni–In LDHs nanosheets with DNA and infrared emissivity study

**Yongjuan Wang · Yuming Zhou · Tao Zhang ·
Man He · Xiaohai Bu**

Abstract The biomolecule–inorganic hybrid materials are potential candidates for low infrared emissivity materials due to the combined functionalities of the biomolecules and the inorganic components. In this study, we describe a facile approach to fabricate DNA/layered double hydroxides (LDHs) nanohybrid by coassembly of exfoliated Ni–In LDHs nanosheets with DNA. In the assembly progress, exfoliated LDHs nanosheets and DNA with different initial DNA/LDHs mass ratio were mixed together, and the DNA intercalated LDHs nanohybrid was obtained only when the input DNA/LDHs mass ratio is ≤0.3 mg/mg. The structure and morphology of as-fabricated hybrid materials were characterized by X-ray diffraction (XRD), UV–Vis absorption spectra, Fourier transform infrared (FT-IR) spectra, thermogravimetry (TG), scanning electron microscopy (SEM), and transmission electron microscopy (TEM). The results indicate that the reassembled product has layered structures incorporated with DNA biomolecule. The nanohybrid with expanding LDHs structure of $d_{003} = 2.6$ nm confirms the intercalation of DNA molecules into the LDHs interlayer. The helix chain oriented parallel to the basal plane of host layer forming ordered sandwich structure. The infrared emissivity value of the DNA/LDHs nanohybrid was then investigated. It was found that the infrared emissivity values were significantly reduced by coassembly of exfoliated LDHs nanosheets with DNA, which may be attributed to the synergistic effect and interfacial interaction between the DNA biomolecule and inorganic LDHs layers reinforced by the construction of ordered sandwich structure.

Introduction

The possibility of cloaking an object from detection by electromagnetic waves has recently become a topic of considerable interest [1]. Low infrared emissivity coatings, concealing the object from infrared detection due to its high infrared reflectivity properties, have attracted great attention [2]. In the past few years, extensive works have been focused on the materials with low infrared emissivity [3–5]. Nanocomposites containing two or more different nanoscale functionalities are attractive candidates for infrared stealth [6–8]. The structure, interface characteristics, and the tunable components of the nanocomposites efficiently affect the infrared emissivity of the materials. Accordingly, a series of low infrared emissivity nanocomposite materials such as inorganic–inorganic [4, 9], organic–inorganic [8, 10], and biomolecule–inorganic [11–13] composites have been developed. Among them the biomolecule–inorganic nanohybrids composed of layered double hydroxides (LDHs) and biomolecules have potential application as low infrared emissivity coatings for the synergistic effect and interfacial interaction between the two components [12].

Recently, the applications of LDHs as low infrared emissivity materials have been studied [12, 14, 15]. The tunable properties and ordered nanostructure of LDHs make them attractive candidates for low infrared emissivity materials. LDHs, also known as hydrotalcite-like materials, are a class of two-dimensional (2D) anionic clays consisting of positively charged host layers and exchangeable

Y. Wang · Y. Zhou (✉) · T. Zhang · M. He · X. Bu
School of Chemistry and Chemical Engineering, Jiangsu
Optoelectronic Functional Materials and Engineering
Laboratory, Southeast University, Nanjing 211189,
People's Republic of China
e-mail: ymzhou@seu.edu.cn

Y. Wang
e-mail: wangyongjuan0630@126.com

interlayer anions, which can be expressed by the formula $[M^{II}_{1-x}M^{III}_x(OH)_2]^{x+}(A^{n-})_{x/n} \cdot yH_2O$ [16]. Due to the specific properties of LDHs such as wide interlayer composition, high and tunable layer charge density, and opened layer structure, LDHs have been used to build different biohybrid systems with biomolecules [17–20]. The positively charged layers are attractive for biomolecules immobilization. It has been reported that macromolecules with ordered secondary structure can significantly reduce the infrared emissivity value due to the formation of massive intermolecular interaction [21]. DNA, as a kind of natural biomolecule, has ordered double helix chains which may be favorable for low infrared emissivity materials. Thus, the coassembly of LDHs and DNA to fabricate the DNA/LDHs nanohybrid may significantly reduce the infrared emissivity values of the materials owing to the combined effect and interfacial interaction between the DNA biomolecule and inorganic LDHs.

Various soft chemistry processes such as ion-exchange [17], delamination/restacking [19], and coprecipitation [20, 22] methods have been used to prepare new biohybrid. The LDHs layers are forever positively charged and surrounded with hydrogen-bonding layers which provide electrostatic-driven hydrophilic surfaces. Based on the negative charges on the surfaces of DNA chain, the assembly of the DNA with LDHs is possible. Jin-Ho Choy and his co-workers have successfully synthesized the DNA intercalated LDHs by anion-exchange method [17, 23]. However, the anion-exchange method is time consuming (shaking about 7 days) and is restricted by the size of the biomolecules. It is not favorable for the intercalation of bulk biomolecules. Herein, we explore a facile, simple, and fast approach to prepare DNA/LDHs nanohybrid by the delamination/restacking method based on the coassembly of the exfoliated LDHs nanosheets with DNA. The microstructure and the morphology of the obtained DNA/LDHs nanohybrids were characterized in detail. The infrared emissivity values of the products were then investigated.

Materials and methods

Materials

Nickel hydroxide and indium hydroxide were obtained from Aladdin Reagent, Shanghai, China. Acetic acid and sodium hydroxide were purchased from Sinopharm Chemical Reagent Co., Ltd., Shanghai, China. Salmon sperm DNA (D1626, approximately 2000 bp) was purchased from the Sigma Chemical Co. All the reagents above were analytical reagent grade and were used without further purification. Deionized and decarbonated water was used in all solutions.

Preparation of exfoliated Ni–In LDHs nanosheets

Typically, 0.2 mol of acetic acid was diluted with 30 mL deionized water, 0.03 mol of nickel hydroxide and 0.01 mol of indium hydroxide were added into the above solution. The mixtures were stirred at 80 °C until a clear and transparent green solution obtained. NaOH solution (4 M) was additionally introduced until the pH of the reaction mixture reached 10. The resulting slurry was sealed in an autoclave and heated at 80 °C for 24 h. The solid was centrifuged, washed thoroughly with deionized water to pH 7. The sample synthesized above was named as Ni–In–CH_3COO^- LDHs. The wet gel was suspended in deionized water and the suspension was laid aside for about 24 h, then a translucent colloidal solution was produced. The content of LDH nanosheets in the colloidal solution is estimated to be 1 mg/mL. The exfoliated LDHs were named as Ni–In ELDHs nanosheets. The whole procedure was carried out under N_2 atmosphere to avoid contamination by atmospheric CO_2. The deionized water for the preparation of all aqueous solutions was decarbonated by boiling prior to use.

### Coassembly of Ni–In ELDHs nanosheets with DNA

For the assembly of Ni–In ELDHs nanosheets with DNA, 20 mL colloidal solution of 1 mg/mL Ni–In ELDHs nanosheets was mixed with 20 mL freshly prepared DNA solution in Tris–HCl buffer (pH 8). The DNA concentration was set as 0.1, 0.15, 0.2, 0.25, 0.3, 0.35, 0.4, 0.5, 1, 2, 3, and 4 mg/mL, corresponding to an input DNA/LDHs mass ratio of 0.1, 0.15, 0.2, 0.25, 0.3, 0.35, 0.4, 0.5, 1, 2, 3, and 4 (mg/mg). The mixture of LDHs nanosheets and DNA were stirred at 50 °C for 12 h until the assembly finished. The precipitate was centrifuged, washed several times with fresh buffer to remove the floating DNA, and then dried.

Characterization

X-ray diffraction (XRD) data were collected by Bruker D8 instrument (Cu K_α radiation, $\lambda = 0.15405$ nm, 40 kV/30 mA). thermogravimetry (TG) curves were carried out with Rigaku ThermoPlus TG8120 at 10 °C/min and under nitrogen flow from 25 to 800 °C. Fourier transform infrared (FT-IR) spectra in the range of 400–4000 cm^{-1} were measured on Nicolet Magna-IR 750 spectrometer (USA) using the KBr pellet technique. UV–Vis spectra were measured on a Shimadzu UV-3600 spectropolarimeter. The morphologies and structure of the samples were examined with a Hitachi S-3400 N a scanning electron microscopy (SEM) and a Hitachi H-600 transmission electron microscopy (TEM). Infrared emissivity values of the samples were carried out on IR-2 Double Band Infrared
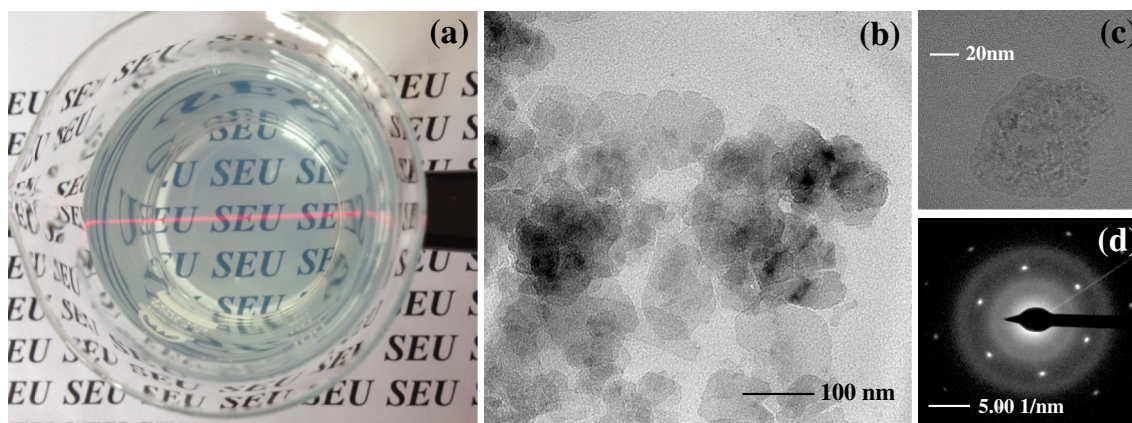
Fig. 1 a Photograph of a colloidal suspension of Ni–In ELDHs nanosheets. The light beam was incident from the side to demonstrate the Tyndall effect. **b, c** TEM images of Ni–In ELDHs nanosheets, **d** the SAED pattern of the nanosheets
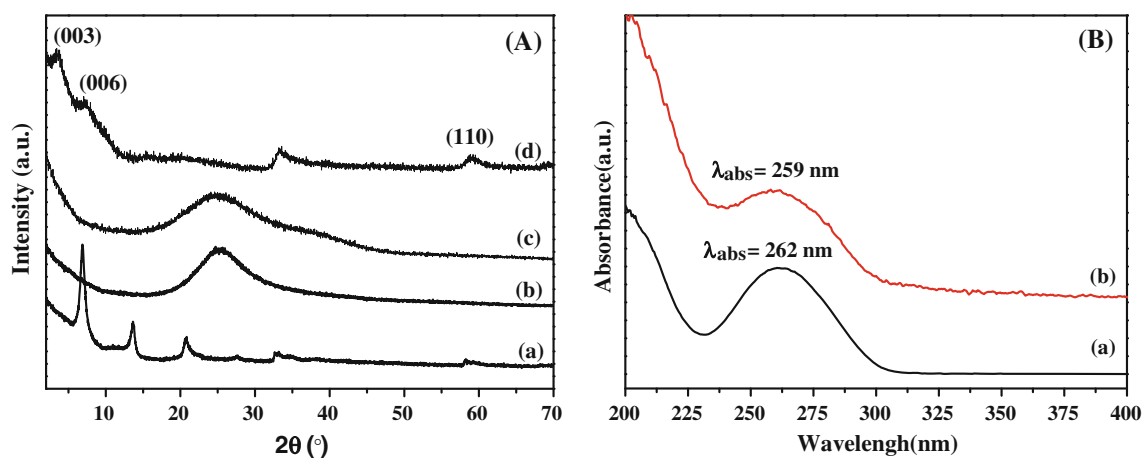
Fig. 2 A XRD patterns of (a) Ni–In–CH₃COO⁻ LDHs, (b) Ni–In ELDHs nanosheets, (c) the DNA/LDHs complex (DNA/LDHs = 4 mg/mg), and DNA/LDHs nanohybrid and **B** UV–vis spectrums of (a) DNA, DNA/LDHs nanohybrid

Emissometer of Shanghai Institute of Technology and Physics, China. Samples were tiled uniformly on round glazed Al slices.

Results and discussion

Preparation of exfoliated Ni–In LDHs nanosheets

In this study, LDHs slabs were colloidized by the delamination of acetate-intercalated Ni–In LDHs in aqueous medium following the coprecipitation procedure. The presence of the exfoliated LDHs layers was first confirmed by the appearance of the Tyndall light scattering when irradiating the colloid with a laser beam (Fig. 1a). The XRD pattern of the wet colloidal aggregate of the exfoliated LDHs nanosheets is displayed in Fig. 2A (b). The sharp basal reflections of the parent Ni–In–CH₃COO⁻

LDHs (Fig. 2A (a)) were absent in this pattern, indicating that the layer structure has collapsed. Instead, a noticeable amorphous-like halo was observed in the 2θ range of 20–30° which is ascribed to the scattering of the water. A similar broad hump has been observed for the other exfoliated LDHs nanosheets [24]. The morphology and local crystal structure of the exfoliated particles were characterized by TEM/SAED analysis. As presented in Fig. 1b, the exfoliated nanosheets show generally plate-like morphologies with weak homogeneous contrast, revealing their uniform nanometric thickness. The HR-TEM image shown in Fig. 1c further confirmed the formation of very thin Ni–In ELDHs nanosheets. The SAED pattern (Fig. 1d) of the exfoliated nanosheets revealed a distinct hexagonal pattern, indicating the maintenance of hexagonal LDHs layers of the parent Ni–In LDHs on delamination. These results provide powerful evidences for the delamination of Ni–In LDHs into ultrathin nanosheets.

Fig. 3 **a** Schematic representation of DNA helix chain, **b** profiles of adsorption amount of DNA on LDHs versus DNA concentration in solution
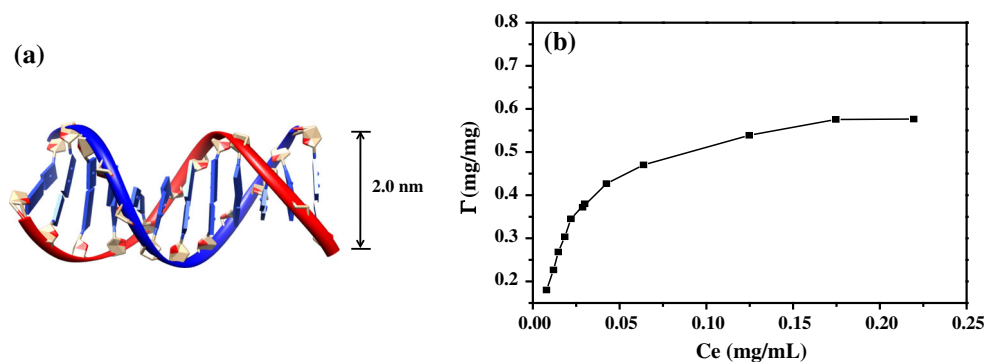

Coassembly of Ni–In ELDHs nanosheets with DNA

In the assembly of Ni–In ELDHs nanosheets with DNA, the acetate anions balancing the positive charge of LDHs layers are to be replaced gradually by the negatively charged DNA through ion exchange. Figure 3a illustrates the structure of DNA with double helix chains. The diameter of the helix chain is about 2.0 nm. The negative charges are concentrated on the backbone of the helix chain. Hence, DNA molecules are supposed to be preferably oriented lying flat on the two-dimensional LDHs surface. Figure 3b displays the profiles of DNA adsorption amount (Γ) versus the steady concentration of DNA in buffer solution (Ce). The DNA adsorption exhibits typical L-shaped change with DNA concentration. As mentioned above, the interfacial assembly requires DNA molecules to gradually replace the acetate anions balancing the charge of LDHs nanosheets. The Langmuir-type adsorptions illustrating that DNA molecules are nearly monolayer adsorbed on the surface of the nanosheets and the adsorbed surface is almost homogeneous which is beneficial for the restacking of the exfoliated nanosheets. However, in the assembly progress, precipitant appears only when the initial DNA/LDHs mass ratio is ≤0.3 mg/mg. The precipitant was collected and characterized and DNA/LDHs nanohybrid mentioned thereafter are all with DNA/LDHs = 0.3 mg/mg. Figure 2A (d) displays the XRD pattern of the DNA/LDHs nanohybrid. A series of (*001*) Bragg peaks can commonly be observed for the as-prepared materials, illustrating the formation of layered LDHs structure. The first peak occurring at a low 2θ angle was attributed to the (*003*) reflection of crystallographic planes of LDHs. It corresponds to the basal repeat distance *d* which equals to the thickness of hydroxide sheet plus the interlayer space that contains the guest anions surrounded by water molecules [25]. Thus, the basal spacing is obtained to be 2.65 nm. Taking the thickness of the LDHs layer (0.48 nm [26, 27]) into account, the interlayer distance of the nanohybrid is estimated to be about 2.17 nm in consistent with the diameter of the DNA helix chain. Consequently, the interlayer gallery could be considered as a monolayer arrangement of DNA molecules since it adopts a helix-oriented parallel to the basal plane of LDHs which is exactly in accordance with the adsorption results discussed above. The appearance of the in-plane (*110*) reflection corresponding to the intermetallic distance within the hydroxide layers further conforms the formation of the LDHs host layers.

While the initial mass ratio of DNA/LDHs is above 0.3 mg/mg, steady colloid suspension is obtained with no sediment. In order to find out the structure of the adsorption complexes with the mass ratio above 0.3 mg/mg, the suspension is centrifuged and the aggregates are characterized. The XRD pattern of the complexes is shown in Fig. 2A (c) which is similar to that of exfoliated LDHs nanosheets (Fig. 2A (b)). No diffraction assigned to the DNA intercalated LDHs was observed, indicating that DNA molecules were adsorbed on the surfaces of the Ni–In ELDHs nanosheets without any aggregation to form the DNA intercalated structures. It is not difficult to understand that both sides of the Ni–In ELDHs nanosheets are positively charged which is proposed to be compensated by the negatively charged DNA molecules. While the initial DNA/LDHs mass ratio is sufficiently high, both sides of the nanosheets are compensated by free DNA molecules before the layer stacking of the nanosheets occurs preventing the coassembly of Ni–In ELDHs nanosheets with DNA. It is demonstrated that the ability of DNA to induce the restacking of exfoliated LDHs nanosheet is relative weak compared with some protein as reported by An et al. [19], for which the layer-restacking took place readily in a wide range of input protein/LDHs mass ratio. The diversity of the interfacial recognition of positively charged LDHs layers to negatively charged biomolecules may be resulting from the different structures and surface charge distribution of the biomolecules.

The UV–Vis absorption spectra of DNA and DNA/LDHs nanohybrid are shown in Fig. 2B. The DNA solution showed an absorption maximum at approximately 260 nm (Fig. 2B (a)), which can be attributed to the typical
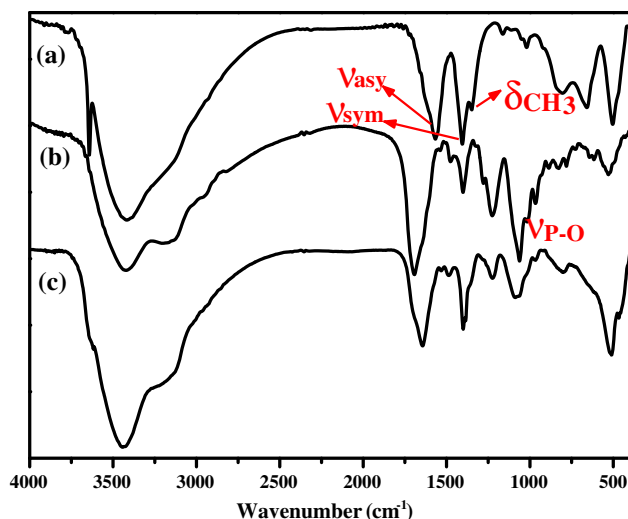
Fig. 4 FT-IR spectrums of (a) Ni–In ELDHs nanosheets, (b) DNA, and (c) DNA/LDHs nanohybrid

$\pi \rightarrow \pi^*$ or $n \rightarrow \pi^*$ transitions in the bases of nucleic acids [17]. The spectra of the prepared DNA/LDHs nanohybrid (Fig. 2B (b)) displayed characteristic absorption band of native DNA. The slightly red-shifted of the adsorption band was resulted from the hybridization indicating that the DNA molecules are hybridized with the hydroxide layers.

Figure 4c shows the FT-IR spectra for the DNA/LDHs nanohybrid. All the characteristic bands, corresponding to DNA molecules, appear with the superimposition on the Ni–In ELDHs nanosheets. First, the absorption bands at 1564 and 1408 cm^{-1} due to the anti-symmetric and symmetric stretching modes of the COO$^-$ group and at 1342 cm^{-1} for the bending mode of the –CH$_3$ group of the acetate anion (Fig. 4a) [28] disappear after the assembly process, suggesting that the CH$_3$COO$^-$ ion was completely replaced by DNA molecule. The absorption bands at 1000–1100 cm^{-1} correspond to the stretching modes of PO$_3^{2-}$ in DNA. Compared with the spectra of the native DNA (Fig. 4b), they are relatively broad owing to the interaction between the DNA molecules and the LDHs host layers [17]. Besides, no new bands are found in the FT-IR spectra of the DNA/LDHs nanohybrid. It is therefore concluded that the negatively charged DNA molecules compensate the positively charged surface of the LDHs nanosheets forming the DNA/LDHs nanohybrids via electrostatic interaction.

The morphology and structure of the DNA/LDHs nanohybrid were characterized by SEM and TEM as presented in Fig. 5. The Ni–In ELDHs nanosheets display well-dispersed plate-like particles (Fig. 1b), whereas the coassembly of the nanosheets with DNA leads to quite different sample morphology. As shown in Fig. 5a and b,

DNA/LDHs nanohybrid exhibits irregular block shape with the plate-like Ni–In ELDHs nanosheets aggregated in assistance of the negatively charged DNA molecules to form the macroscopic layered structure. The microscopic structure of the nanohybrid is then investigated by TEM images. As displayed clearly in Fig. 5c and d, layered sandwich structure was formed by alternating the DNA helix chains (in light color) and LDHs host layers (in black color). The basal spacing measured from the TEM image was about 2.6 nm quite in consistence with the XRD analysis further confirming the horizontal orientation of the DNA helix chain in the gallery of LDHs host layers.

Scheme 1 is a schematic model proposed for the coassembly process according to the above results. First, Ni–In ELDHs nanosheets are obtained by the delaminating of Ni–In–CH$_3$COO$^-$ LDHs on the action of water which are described elsewhere by our group. After exfoliation, the acetate anions still adsorb on the surface of the Ni–In ELDHs nanosheets in order to balance the positive charges of the LDHs layers (evidenced by the FT-IR spectra in Fig. 4a). As discussed above, the acetate anions balancing the positive charge of LDHs layers are replaced gradually by the negatively charged DNA through ion exchange in the assembly process. Since the ability of DNA to induce the layer stacking of LDHs nanosheets is relative weak, the restacking of the exfoliated nanosheets occurs only when the input DNA/LDHs mass ratio is ≤0.3 mg/mg. After the total restack of the nanosheets, the construction of the DNA/LDHs nanohybrid with layered structure was completed. For the negative charges are concentrated on the backbone of the helix chain of DNA, the DNA molecules oriented parallel to the basal plane of LDHs host layer to form the ordered sandwich structure.

Thermal analysis

TG curves of pure DNA, Ni–In–CH$_3$COO$^-$ LDHs, and DNA/LDHs nanohybrids are shown in Fig. 6. DNA (Fig. 6a) displays three mass loss over the temperature ranges 25–220 °C, 220–350 °C, and above 350 °C. The weight loss below 220 °C is attributed to the evaporation of physically adsorbed water. The weight loss above 220 °C is attributed to the total result of the thermal degradation and decomposition. The thermal behavior of Ni–In–CH$_3$COO$^-$ LDHs is plotted in Fig. 6b. The weight decrease at 25–158 °C is assigned as the removal of the surface-adsorbed water molecules. The weight loss appeared at 158–212 °C could be mainly attributed to the removal of interlayer water molecules. The weight loss at 212–332 °C is attributed to the thermal decomposition of brucite-like layers through the removal of OH groups in the form of water molecules. The weight loss in the range 332–498 °C is ascribed to total results of the dehydroxylation of the

Fig. 5 a, **b** SEM images and **c**, **d** TEM images of DNA/LDHs nanohybrids
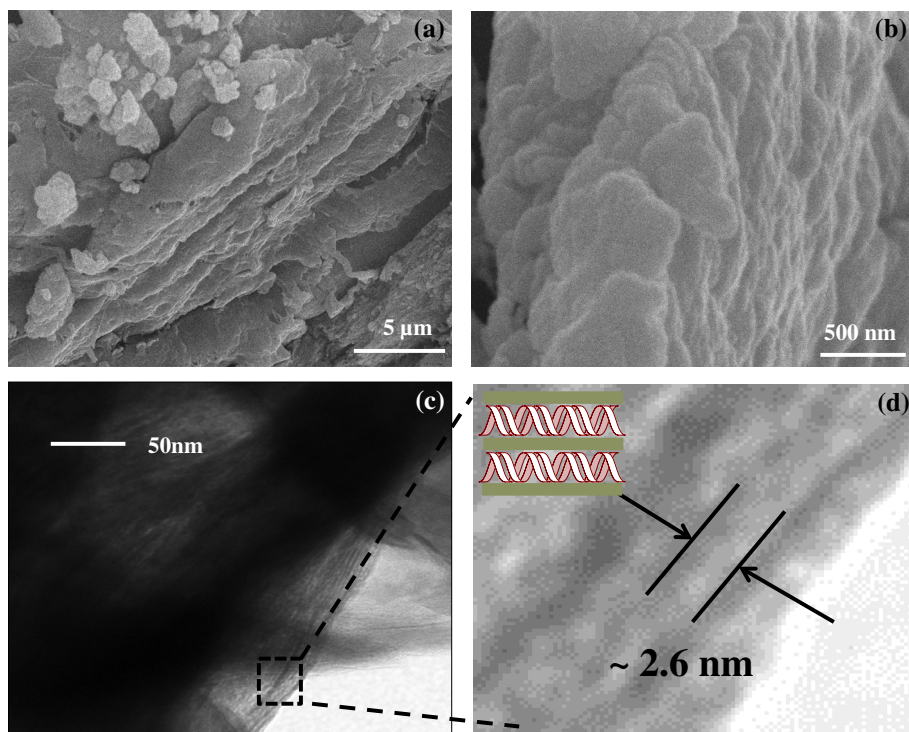
**Scheme 1** Sketch presentation of the formation process of DNA/LDHs nanohybrid
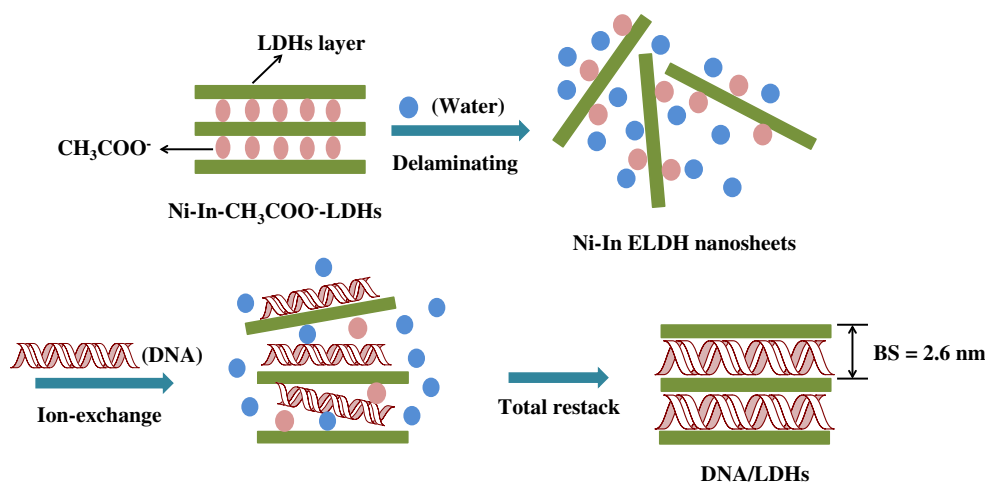
layers and the decomposition of the intercalated acetate anions. There was no obvious weight loss above 500 °C, demonstrating that the phase transformation from the LDHs to metal oxide was completed.

Part c of Fig. 6 is the curve of DNA/LDHs nanohybrids. The weight loss from 25 to 180 °C is resulted from the evaporation of physically adsorbed water, while the weight loss from 180 to 280 °C is related to the removal of interlayer water molecules. The weight loss between 280 and 390 °C is attributed to the dehydroxylation of the LDHs layers and the partial degradation of DNA. The weight loss from 390 to 800 °C is related to the further degradation and decomposition of DNA. Generally

speaking, the starting degradation temperature of native DNA and LDHs are 220 and 212 °C, respectively, while the degradation of DNA/LDHs nanohybrids start from 280 °C. Therefore, the thermal stability of the materials is improved by the coassembly of DNA and Ni–In ELDHs nanosheets.

Infrared emissivity study

The infrared emissivity values of the samples at wavelength of 8–14 μm are investigated at room temperature and shown in Table 1. The infrared emissivity value of Ni–In–CH_3COO^- LDHs is 0.705, lower than that of other
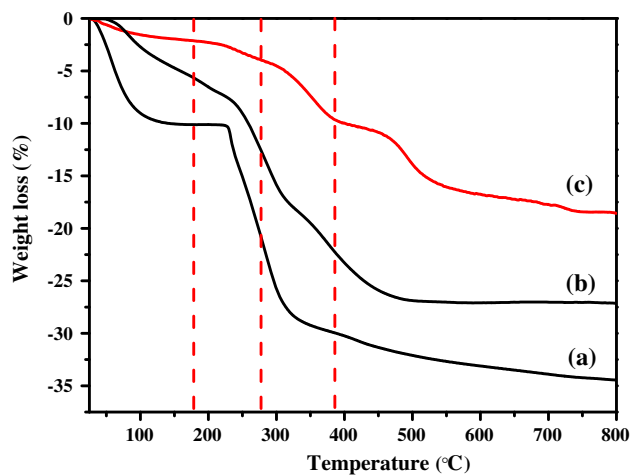
Fig. 6 TG diagrams of (a) DNA, (b) Ni–In–CH$_3$COO$^-$ LDHs, and (c) DNA/LDHs nanohybrids

Table 1 Infrared emissivity of samples

Samples	Infrared emissivity (ε_{TIR} at 8–14 μm)
Ni–In–CH$_3$COO$^-$ LDHs	0.705
DNA	0.802
DNA/LDHs mixture	0.739
DNA adsorbed LDHs complex	0.673
DNA/LDHs nanohybrid	0.528

The DNA/LDHs mixture was prepared by directly mixing of DNA and Ni–In–CH$_3$COO$^-$ LDHs and DNA adsorbed LDHs complex was obtained by DNA adsorption on Ni–In–CH$_3$COO$^-$ LDHs at 25 °C for 12 h. DNA/LDHs = 0.3 mg/mg for DNA/LDHs mixture, DNA adsorbed LDHs complex and DNA/LDHs nanohybrid

LDHs, as studied before by our group [15]. DNA has an infrared emissivity value of 0.802. It is well known that organic polymers have high infrared emissivity values due to their high unsaturated groups in the structure. The ordered secondary structure of macromolecule chain results in the formation of massive intermolecular interaction, which reduces the index of hydrogen deficiency and the unsaturated degree [21]. Consequently, the infrared emissivity value of DNA biomolecule with natural ordered double helix chains is relatively lower than common molecules [29].

When DNA is directly mixed with unexfoliated Ni–In–CH$_3$COO$^-$ LDHs, the infrared emissivity reduced to 0.739 which is ascribed to the simply co-effect of the two components. While DNA is adsorbed on the surface of the LDHs, the infrared emissivity of the DNA adsorbed LDHs complex is 0.673 lower than the value of the DNA/LDHs mixture. The decrease of the value may be attributed to the interfacial interaction enhanced by the vander Waals,

hydrogen bonding and electrostatic forces present between DNA and LDHs through the adsorption process. The infrared emissivity value of DNA/LDHs nanohybrids is 0.528 further reduced by the intercalation of DNA in the gallery of LDHs host layer. When DNA is assembled with the exfoliated nanosheets, the backbone of the DNA chain is oriented parallel to the basal plane of the LDHs host layer to form ordered sandwich structure as discussed above. The interfacial interaction was reinforced by the construction of the ordered sandwich structure. The geometrically constrained environment supplied by LDHs host alter the vibration mode of the atoms or pendant groups on the interface between DNA and LDHs host layers, which directly reduced the infrared emissivity value of the material.

Conclusion

The DNA/LDHs nanohybrid was prepared by the coassembly of the delaminated Ni–In LDHs nanosheets with DNA and the infrared emissivity values of the samples at wavelength of 8–14 μm were investigated. The obtained DNA/LDHs nanohybrid has ordered sandwich structure with the DNA helix chain oriented parallel to the basal plane of the positive LDHs host layer. The thermal stability of the materials was improved by the coassembly of DNA with LDHs nanosheets. The infrared emissivity value of the nanohybrids was low attributed to the synergistic effect between DNA and the host layer of LDHs. This work not only presents a facile, simple, and convenient method for the fabrication of DNA/LDHs nanohybrid, but also provides an opportunity for developing new infrared low-emissive materials.

References

1. Liu R, Ji C, Mock J et al (2009) Broadband ground-plane cloak. Science 323:366–369
2. Chou KS, Lu YC (2007) The application of nanosized silver colloids in far infrared low-emissive coating. Thin Solid Films 515:7217–7221
3. Chen L, Lu C, Fang Z et al (2013) Infrared emissivity and microwave absorption property of Sm$_{0.5}$Sr$_{0.5}$CoO$_3$ perovskites decorated with carbon nanotubes. Mater Lett 93:308–311
4. Su X, Liu X, Jia Y et al (2013) Effect of synthesized temperature on microstructure, infrared emissivity and dielectric property of Fe-doped ZnO powder. J Mater Sci Mater Electron 24:4974–4979

5. Sun K, Zhou W, Tang X et al (2012) Effects of air annealing on the structure, resistivity, infrared emissivity and transmission of indium tin oxide films. Surf Coat Technol 206:4095–4098

6. Bu X, Zhou Y, He M et al (2014) Fabrication and characterization of optically active polyacetylene@WO3 nanorod hybrids with low infrared emissivity. Mater Lett 120:239–242

7. Zhang W, Xu G, Ding R et al (2013) Microstructure, optimum pigment content and low infrared emissivity of polyurethane/Ag composite coatings. Phys B 422:36–39

8. Zhang W, Xu G, Ding R et al (2013) Nacre biomimetic design—a possible approach to prepare low infrared emissivity composite coatings. Mater Sci Eng C 33:99–102

9. Fu LS, Jiang JT, Zhen L et al (2013) FeNi$_3$/indium tin oxide (ITO) composite nanoparticles with excellent microwave absorption performance and low infrared emissivity. Mater Sci Eng B 178:225–230

10. Yan X, Xu G (2012) Influence of silane coupling agent on corrosion-resistant property in low infrared emissivity Cu/polyurethane coating. Prog Org Coat 73:232–238

11. Ye X, Zhou Y, Sun Y et al (2008) Structure and infrared emissivity of collagen/SiO$_2$ composite. Appl Surf Sci 254:5975–5980

12. Sun Y, Zhou Y, Ye X et al (2008) Fabrication and infrared emissivity study of hybrid materials based on immobilization of collagen onto exfoliated LDH. Mater Lett 62:2943–2946

13. Cao Y, Zhou YM, Shan Y et al (2005) Preparation and characterization of grafted collagen confined in mesoporous silica. Chin J Inorg Chem 21:331–336

14. Zhu Y, Zhou Y, Zhang T et al (2012) Preparation and characterization of lactate-intercalated Co–Fe layered double hydroxides and exfoliated nanosheet film with low infrared emissivity. Appl Surf Sci 263:132–138

15. Wang Y, Zhou Y, Zhang T et al (2014) Acetate-intercalated Ni–In layered double hydroxides with low infrared emissivity: synthesis, delamination and restacked to form the multilayer films. Appl Surf Sci 288:710–717

16. Evans D, Slade R (2006) Structural aspects of layered double hydroxides layered double hydroxides. Springer, Berlin, pp 1–87

17. Choy JH, Kwak SY, Park JS et al (1999) Intercalative nanohybrids of nucleoside monophosphates and DNA in layered metal hydroxide. J Am Chem Soc 121:1399–1400

18. Chen X, Fu C, Wang Y et al (2008) Direct electrochemistry and electrocatalysis based on a film of horseradish peroxidase intercalated into Ni–Al layered double hydroxide nanosheets. Biosens Bioelectron 24:356–361

19. An Z, Lu S, He J et al (2009) Colloidal assembly of proteins with delaminated lamellas of layered metal hydroxide. Langmuir 25:10704–10710

20. Charradi K, Forano C, Prevot V et al (2010) Characterization of hemoglobin immobilized in MgAl-layered double hydroxides by the coprecipitation method. Langmuir 26:9997–10004

21. Yang Y, Zhou Y, Ge J et al (2011) Synthesis, characterization and infrared emissivity property of optically active polyurethane derived from tyrosine. Polymer 52:3745–3751

22. Yasutake A, Aisawa S, Takahashi S et al (2008) Synthesis of biopolymer intercalated inorganic-layered materials: intercalation of collagen peptide and soybean peptide into Zn–Al layered double hydroxide and layered zinc hydroxide. J Phys Chem Solids 69:1542–1546

23. Choy JH, Kwak SY, Jeong YJ et al (2000) Inorganic layered double hydroxides as nonviral vectors. Angew Chem Int Ed 39:4041–4045

24. Hibino T, Jones W (2001) New approach to the delamination of layered double hydroxides. J Mater Chem 11:1321–1323

25. Rives V (2001) Layered double hydroxides: present and future. Nova Science Publication, New York

26. Khan AI, O'Hare D (2002) Intercalation chemistry of layered double hydroxides: recent developments and applications. J Mater Chem 12:3191–3198

27. Xu ZP, Braterman PS (2003) High affinity of dodecylbenzene sulfonate for layered double hydroxide and resulting morphological changes. J Mater Chem 13:268–273

28. Nakamoto K (2006) Infrared and Raman spectra of inorganic and coordination compounds. Wiley, New Jersey

29. Wang Z, Zhou Y, Sun Y (2010) Helical polyurethane-imide@attapulgite composite: preparation, characterization and infrared emissivity study. Mater Lett 64:908–911